

Conical Diffraction from Approximate Dirac Cone States in a Superhoneycomb Lattice

Yongfeng Kang, Hua Zhong, Milivoj R. Belić, Yiqing Tian, Kaichao Jin, Yanpeng Zhang, Fuli Li, and Yiqi Zhang*

Superhoneycomb lattice is an edge-centered honeycomb lattice that represents a hybrid fermionic and bosonic system. It contains pseudospin-1/2 and pseudospin-1 Dirac cones, as well as a flat band in its band structure. In this paper, we cut the superhoneycomb lattice along short-bearded boundaries and obtain the corresponding band structure. The states very close to the Dirac points represent approximate Dirac cone states that can be used to observe conical diffraction during light propagation in the lattice. In comparison with the previous literature, this research is carried out using the continuous model, which brings new results and is simple, direct, accurate, and computationally efficient.

1. Introduction

Recently, a family of two-dimensional (2D) photonic lattices has been introduced, which display interesting energy band structures.^[1–4] Lattices with more than one type of Dirac cone states may exhibit curious novel physical phenomena, like conical diffraction, pseudospin-mediated vortices, beam localization, and Klein tunneling.^[5–10] Among different lattices, the honeycomb and Lieb lattices have stirred a lot of interest, since they play an important role in motivating and clarifying intriguing properties of novel photonic structures.^[11–16] In the previous research it has been displayed that the superhoneycomb lattice combines

the honeycomb and the Lieb lattice and displays the properties of both. It contains two different kinds of Dirac cones, with an intriguing consequence that the superhoneycomb lattice represents a hybrid fermionic and bosonic system.^[17,18] The first two bands as well as the last two bands in the superhoneycomb lattice intersect at a set of diabolic points at six corners of the first Brillouin zone, forming Dirac cones. Such Dirac cones are of the pseudospin-1/2 type. At the same time, other Dirac points, located at the intersection of the flat and other bands correspond to the

pseudospin-1 type. Thus, the system represents a rare but fascinating hybrid fermionic and bosonic physical system.

A key feature related to conical diffraction is the existence of Dirac cones in the band structure. Not all photonic lattices support conical diffraction but only those with Dirac cones that depend on the symmetry of the structure. In the vicinity of a Dirac cone, the dispersion is nearly linear, which indicates that the first-order derivative of the energy band is constant and the second-order derivative is zero. This means that the radius of the beam which excites the Dirac cone state will linearly grow with the propagation distance and give rise to the conical diffraction. Thus far, the related topic has been widely investigated in the honeycomb lattice,^[19] Lieb lattice,^[20] and the edge-centered square lattice,^[10,21–23] to name a few. It is also worth mentioning that the Dirac cones associated with different pseudospins can be observed through mediated vortex generation, which is indicated in the formation mechanism of conical diffraction.^[8,9,18]

We notice that in the previous literature, conical diffraction in superhoneycomb and honeycomb lattices was obtained based on the tight-binding method. Based on the continuous model, in principle one can excite the Dirac cone state by using Gaussian beams that are shifted relative to the Dirac points in the inverted space. However, these Gaussian beams will inevitably excite the bulk states as well. In a direct method, one can calculate the Dirac cone state first and then use such a state as incident, to observe conical diffraction. But, for the superhoneycomb lattice as well as the honeycomb lattice, the first Brillouin zone is not square, and one has to manage very tricky mathematical procedures that involve coordinate transformations several times. So, how to obtain a clean conical diffraction based on the continuous model is still an open problem, ready to be investigated more thoroughly. We have already introduced one effective method to excite Dirac cone states and observe conical diffraction.^[23] Such a method does not

Dr. Y. F. Kang, H. Zhong, Y. Q. Tian, K. C. Jin, Prof. Y. P. Zhang,

Dr. Y. Q. Zhang

Key Laboratory for Physical Electronics and Devices of the Ministry of

Education & Shaanxi Key Lab of Information Photonic Technique

School of Electronic Science and Engineering

Xi'an Jiaotong University

Xi'an 710049, China

E-mail: zhangyiqi@mail.xjtu.edu.cn

H. Zhong, Prof. F. L. Li, Dr. Y. Q. Zhang

Department of Applied Physics

School of Science

Xi'an Jiaotong University

Xi'an 710049, China

H. Zhong, K. C. Jin, Dr. Y. Q. Zhang

Guangdong Xi'an Jiaotong University Academy

Foshan 528300, China

Prof. M. R. Belić

Science Program

Texas A&M University at Qatar

P.O. Box 23874 Doha, Qatar

 The ORCID identification number(s) for the author(s) of this article can be found under <https://doi.org/10.1002/andp.201900295>

DOI: 10.1002/andp.201900295

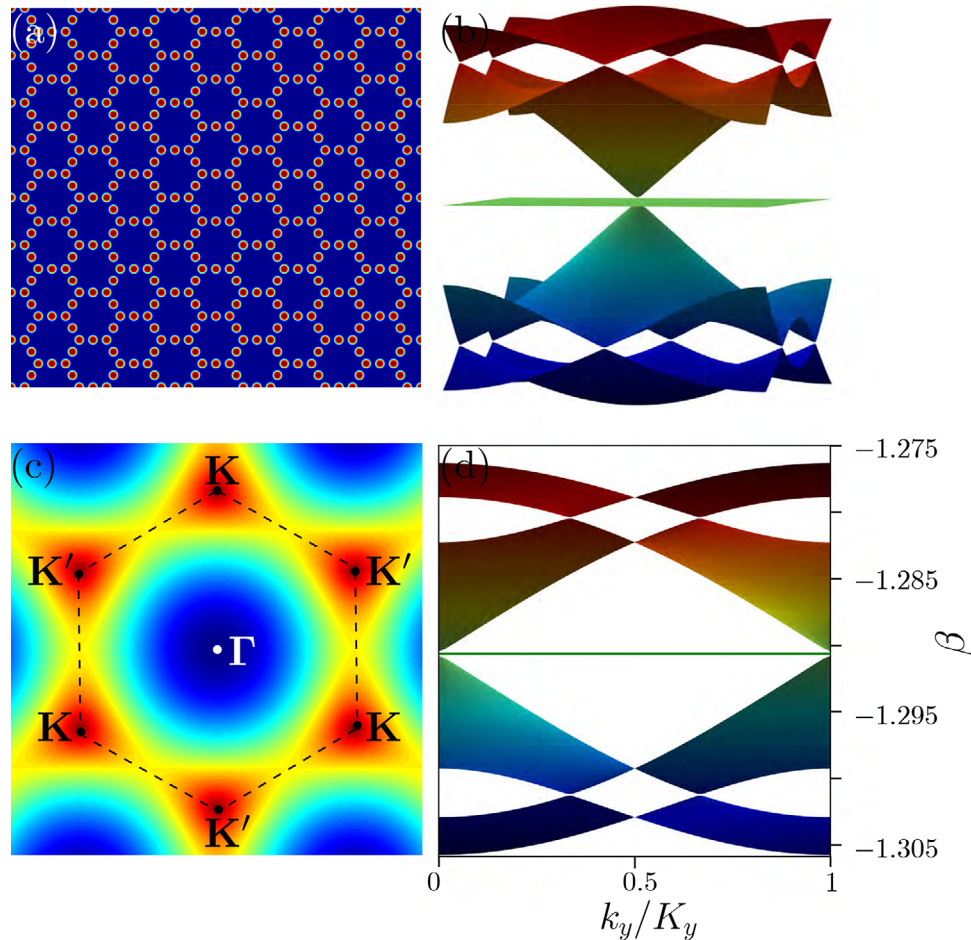


Figure 1. a) The geometry of superhoneycomb lattice. b) 2D band structure. c) First Brillouin zone with high symmetry points. d) Side view of the band structure in (k_y, β) plane. We shift the band structure along k_y direction to set it in the region $k_y \in [0, K_y]$.

rely on the mathematical transformations and is also quite direct. In this paper, we will use this method to investigate conical diffraction in the superhoneycomb lattice, based on the continuous model.

2. Superhoneycomb Lattice Band Structure and States

The propagation of a laser beam in photorefractive crystals can be described by the Schrödinger-like paraxial wave equation that can be written as^[24]:

$$i \frac{\partial \psi(x, y, z)}{\partial z} = -\frac{1}{2k_0} \left(\frac{\partial^2}{\partial x^2} + \frac{\partial^2}{\partial y^2} \right) \psi(x, y, z) - \frac{k_0 \Delta n(x, y)}{n_0} \psi(x, y, z) \quad (1)$$

where $\psi(x, y, z)$ is the envelope of the light beam during propagation and x, y , and z are the transverse and longitudinal coordinates, respectively. Further, $k_0 = 2n_0\pi/\lambda_0$ is the wave number, with the wavelength chosen as $\lambda_0 = 532$ nm. We take an SBN

crystal as an example, with $n_0 = 2.35$ as the ambient refractive index and with Δn as the refractive index change, defined as

$$\Delta n(x, y) = -\frac{1}{2} n_0^3 \gamma_{33} E_0 \frac{1}{1 + I(x, y)} \quad (2)$$

where the bias field is $E_0 = 1$ kV cm⁻¹, the electro-optic coefficient $\gamma_{33} = 280$ pm V⁻¹, and $I(x, y)$ is the intensity pattern which will induce a superhoneycomb lattice in the SBN crystal, through

$$I(x, y) = \left| \sum_{m,n} a \exp \left(-\frac{(x - x_{m,n})^2 + (y - y_{m,n})^2}{w^2} \right) \right|^2 \quad (3)$$

In principle, $I(x, y)$ should stand for the total intensity, which should include the diffracted intensity and the incident beam intensity $|\psi|^2$, but in practice, for computational convenience and for avoiding to deal with a strongly nonlinear system, simplifying assumptions are often made.^[10,24] Here, a represents the beam amplitude, $(x_{m,n}, y_{m,n})$ is the beam center with (m, n) being integers, and w determines the beam width. The distance between two next-nearest-neighbor lattice sites is taken as $d = 60$ μ m, and $w = 0.72$ μ m. The geometry is presented in **Figure 1**.

In Figure 1a, the superhoneycomb lattice induced in the SBN crystal is shown. We would like to note that we take the SBN crystal^[25–33] as our target system; however, our research can be simply extended to other systems, e.g., femto-second laser direct-writing waveguide arrays,^[2,13,34–36] cold atoms,^[37,38] atomic vapors,^[39,40] and exciton-polaritons,^[41–48] to name a few.

For convenience, we transform Equation (1) into a dimensionless equation by replacing x , y , and z with xr_0 , yr_0 , and zL_z , where $L_z = k_0 r_0^2$ is the Rayleigh range. Here, r_0 represents the typical width of the real incident beam. So, we obtain

$$i \frac{\partial \psi(x, y, z)}{\partial z} = -\frac{1}{2} \left(\frac{\partial^2}{\partial x^2} + \frac{\partial^2}{\partial y^2} \right) \psi(x, y, z) - \frac{k_0^2 r_0^2 \Delta n(x, y)}{n_0} \psi(x, y, z) \quad (4)$$

Similar to the honeycomb lattice, there is no single site in one unit cell, and the two unit vectors are not orthogonal to each other.^[7] The two vectors can be written as $\mathbf{v}_1 = (3d, \sqrt{3}d)$ and $\mathbf{v}_2 = (3d, -\sqrt{3}d)$, with the angle between them being $\pi/3$. To calculate the band structure, we first rotate the frame from (x, y) to (X, Y) through the relation

$$\begin{bmatrix} X \\ Y \\ Z \end{bmatrix} = \begin{bmatrix} \cos(\theta) & -\sin(\theta) & 0 \\ \sin(\theta) & \cos(\theta) & 0 \\ 0 & 0 & 1 \end{bmatrix} \begin{bmatrix} x \\ y \\ z \end{bmatrix}$$

with $\theta = \pi/6$. The two vectors become $\mathbf{V}_1 = (2\sqrt{3}d, 0)$ and $\mathbf{V}_2 = (\sqrt{3}d, 3d)$, and the angle between them is still $\pi/3$. Then, we transform the lattice into the frame (x', y') through the relation

$$\begin{bmatrix} X \\ Y \\ Z \end{bmatrix} = \begin{bmatrix} 1 & \cos(\varphi) & 0 \\ 0 & \sin(\varphi) & 0 \\ 0 & 0 & 1 \end{bmatrix} \begin{bmatrix} x' \\ y' \\ z' \end{bmatrix}$$

with $\varphi = \pi/3$. Now, the two unit vectors become $\mathbf{v}'_1 = (2\sqrt{3}d, 0)$ and $\mathbf{v}'_2 = (0, 2\sqrt{3}d)$, which are orthogonal in the frame (x', y') . According to the transforming relations, Equation (4) can be rewritten as:

$$i \frac{\partial \psi(x, y, z)}{\partial z} = -\frac{2}{3} \left(\frac{\partial^2}{\partial x'^2} + \frac{\partial^2}{\partial y'^2} - \frac{\partial^2}{\partial x' \partial y'} \right) \psi(x, y, z) - \frac{k_0^2 r_0^2 \Delta n(x, y)}{n_0} \psi(x, y, z) \quad (5)$$

In Equation (5), we have replaced (x', y', z') by (x, y, z) , which is the usual representation.

We aim to solve Equation (5) presuming the solution in the form $\psi(x, y, z) = u(x, y) \exp(i\beta z)$, with β being the propagation constant that will define different bands. Substituting this solution into the equation, one obtains the following eigenvalue

problem,

$$\beta u(x, y) = \frac{2}{3} \left(\frac{\partial^2}{\partial x^2} + \frac{\partial^2}{\partial y^2} - \frac{\partial^2}{\partial x \partial y} \right) u(x, y) + \frac{k_0^2 r_0^2 \Delta n(x, y)}{n_0} u(x, y) \quad (6)$$

Equation (6) is solved using the plane-wave expansion method, to obtain the corresponding band structure shown in Figure 1b. We label the five bands in Figure 1b as β_1 – β_5 from top to bottom, which includes a flat band β_3 in the middle of the band structure. In the first two bands β_1 and β_2 and the last two bands β_4 and β_5 , there are six Dirac cones that reside at the corners of the first Brillouin zone. Since these Dirac cones are associated with the fermionic system, we define them as Type-F Dirac cones.

At the intersection of the β_2 and β_4 bands, another kind of Dirac cone is obtained, which is related to the bosonic system and therefore, we define it as a Type-B Dirac cone. Clearly, Type-F and Type-B Dirac cones are corresponding to the pseudospin-1/2 and pseudospin-1^[17,18] systems, respectively. In Figure 1c, we show the first Brillouin zone marked with a dashed hexagonal with high symmetric points \mathbf{K} , \mathbf{K}' , and Γ . To show the band structure more clearly, we also project the band structure onto the (k_y, β) plane, as shown in Figure 1d, but in the region $k_y \in [0, K_y]$.

It is well known that the first-order derivatives $d\beta/dk_x$ and $d\beta/dk_y$ of the band structure correspond to the velocity components of the states during propagation, and the second-order derivatives $d^2\beta/dk_x^2$ and $d^2\beta/dk_y^2$ are the corresponding dispersions. The incident beam that excites the flat band will remain unchanged during propagation, and the excited states of the Dirac cone will display conical diffraction.^[18] However, it is not easy to obtain the Dirac cone state directly due to the complex mathematical transformations above, because one has to do inverse transformations. Therefore, we do not adopt such a method to obtain the Dirac cone state, but take a relatively simple method to approach the Dirac cone state.

We assume that the lattice is periodic in the y direction and truncated along the x direction, with the short-bearded boundaries; the geometry of the truncated superhoneycomb lattice is shown in **Figure 2**. The upper right panel of Figure 2 shows the truncated lattice and the related band structure is shown in the left panel. Here, $K_y = 2\pi/D_y$, with $D_y = \sqrt{3}d$. The band structure is quite similar to that shown in Figure 1d, except that there are edge states between the upper two and the bottom two bands. Considering the position of the Dirac cones, we show the states in the right panels of Figure 2, which correspond to different markers placed in the band structure to the left. Since the states are at the interface of the bulk and edge states, the light energy occupies almost all the lattice sites. Taking the upper two states as an example, one finds that the light intensity profiles at the boundaries are almost the same but quite different in the bulk. The similarity and the difference come from the degenerated edge states and different bulk states (different in the β_1 and β_2 bands), respectively. We believe that the states shown in Figure 2 are quite close to the Dirac cone states, and conical diffraction can be easily observed if they are taken as incident.

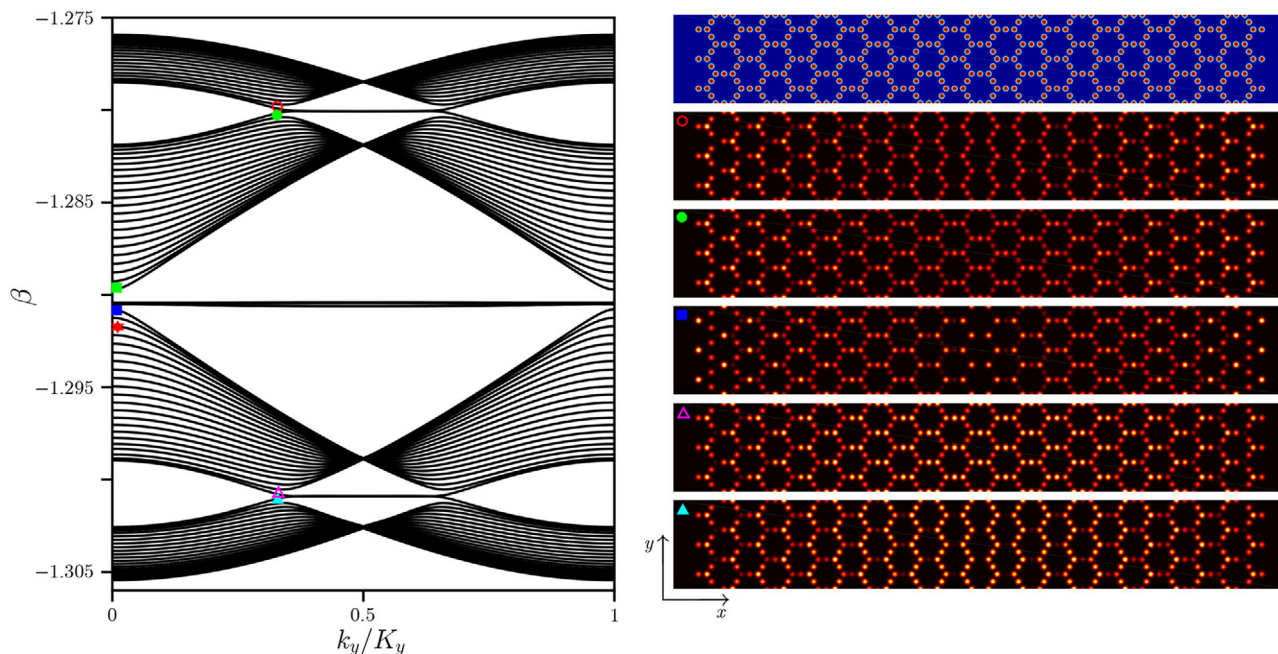


Figure 2. Band structure (left panel) of the truncated superhoneycomb lattice with short-bearded boundaries (right-top panel), and state intensity profiles (right-bottom panels) corresponding to the markers in the band structure.

3. Conical Diffraction

Now, we check the propagation of such approximate Dirac cone states, obtained in Section 2, and try to form a comprehensive understanding of conical diffraction in the superhoneycomb lattice. As the first step, we choose the Type-F Dirac cone state (the red hollow circle marked in Figure 2), superposed with a wide Gaussian beam as the incident, and the beam intensity distributions at selected normalized distances are drawn in **Figure 3a1–a3**. One finds that conical diffraction indeed appears during propagation, which demonstrates that the Dirac cone state is well excited. The input beam is a solid circle at the initial place [Figure 3a1], and it spreads linearly along radial direction during propagation, to form a ring-like structure with a constant thickness,^[49] as shown in Figure 3a2, a3.

One also notes that there appears a notch without beam intensity at the bottom of the ring structure, symmetric about the $x = 0$ line. The appearance of the notch is due to the fact that only one Dirac cone state is excited, which is different from the notch appearance in a honeycomb lattice reported previously in ref. [7,10]. If Gaussian beams are used to excite the Dirac state, a pair of states (marked with red hollow and green solid circles in Figure 2) could be excited simultaneously, without notches in the conical diffraction. As a result, one could predict that if the approximate Dirac cone state marked with the green solid circle in Figure 2 is launched, a conical diffraction will still form, but with a notch appearing on the top of the ring. The corresponding numerical simulation is exhibited in Figures 3b1–b3, which verifies the prediction.

Now, it is natural to suggest exciting the Dirac cone states by using the states marked with red hollow and green solid circles in Figure 2 simultaneously, and obtain a conical diffraction without

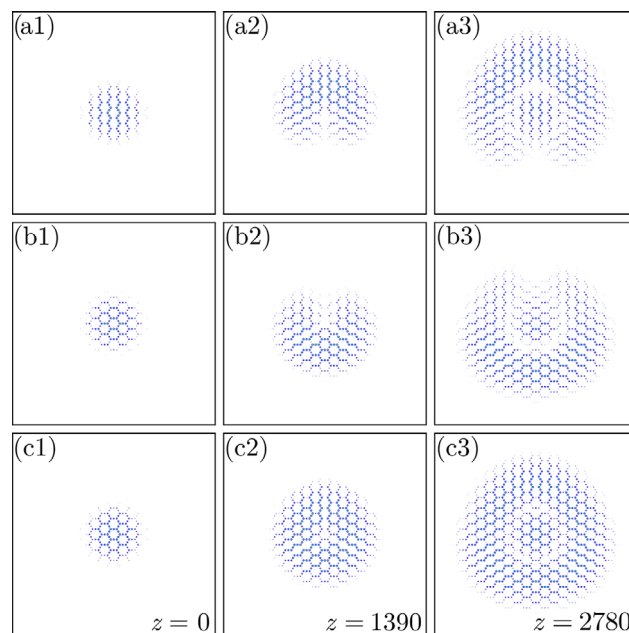


Figure 3. Beam intensity at different distances during propagation, displaying the formation of conical diffraction. The propagation distance is shown in the right-bottom corner of each panel. a) Diffraction of the Dirac state marked by the red hollow circle in Figure 2, multiplied by a Gaussian envelope. The input beam transforms into a ring with two bright rings of constant thickness. b) Setup is as in (a), but for the state marked by a green solid circle in Figure 2. c) Combination of the intensity profiles in (a) and (b). The panels are shown in the window $-139 \leq x \leq 139$, $-139 \leq y \leq 139$.

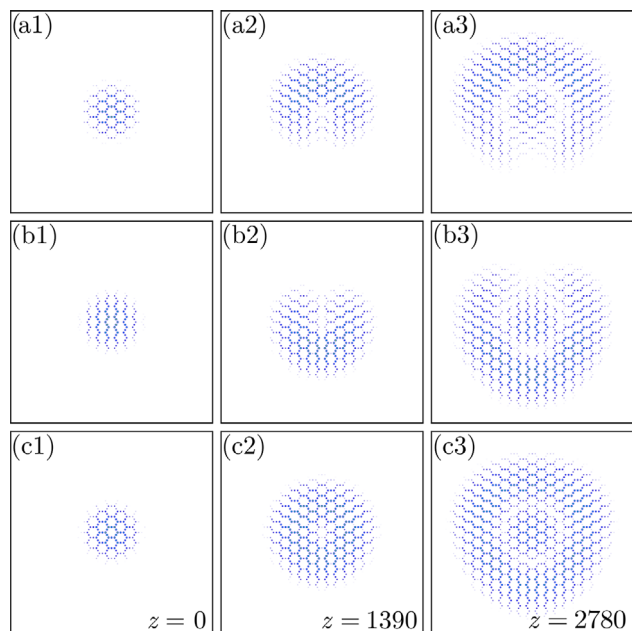


Figure 4. Figure setup is as Figure 3, but for the states marked with triangles in Figure 2

a notch. However, a simple superposition of the two approximate Dirac cone states will not help reach such a goal definitely. The reason is due to the limitation of the eigenvectors obtained based on the eigenvalue problem, which are gauge-independent, and the phase difference among the states is not fixed, which could be π , $\pi/2$, or something else. Therefore, we only consider the amplitude of the states and add them simply; the results are displayed in Figure 3c1–c3. One finds that the conical diffraction ring is complete and intensity is uniform along the ring.

Taking the same procedure, we proceed to study the conical diffraction of the approximate Dirac cone states that are marked by the magenta hollow and azure solid triangles in Figure 2. The numerical results are presented in **Figure 4**, which is in the same setup as Figure 3. Clearly, one finds that the results in Figure 4 are quite similar to those in Figure 3. For the beam which excites the Dirac cone state marked with the magenta hollow triangle in Figure 2, conical diffraction is with a notch at the bottom of the ring, as shown in Figure 4a1–a3. While if the beam excites the state marked with the cyan solid triangle, conical diffraction is with a notch at the top of the ring, as Figure 4b1–b3 display. In Figure 4c1–c3, a complete conical diffraction ring is observed if the amplitudes of the conical diffractions with notches are combined.

It is worth mentioning that in the superhoneycomb lattice, Type-F Dirac points contain two inequivalent Dirac cones at the \mathbf{K} and \mathbf{K}' points. The results obtained in the above investigation are at the \mathbf{K} points [please see Figure 1c]. For the conical diffraction at \mathbf{K}' points, we can also get the analogous results, but the notches in the conical diffraction during propagation will be opposite to those of the \mathbf{K} points, which can be viewed as the mirror process of the one at the \mathbf{K} points, which is proven in ref. [23]. For the sake of brevity, we do not show the results associated with the \mathbf{K}' points in the paper.

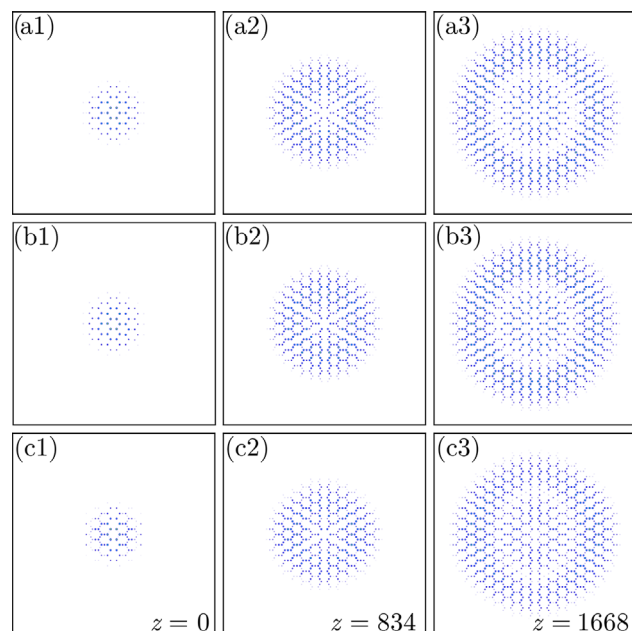


Figure 5. a1–a3) Conical diffraction of the state marked with a blue solid square in Figure 2. b1–b3) Setup is as (a1)–(a3), but for the state marked with a green solid square. c1–c3) Setup is as (a1)–(a3), but for the state marked with a red solid star.

As a comparison with the conical diffraction from Type-F Dirac cones, utilizing the same approach, we investigate the conical diffraction from the Type-B Dirac cones. Since the Dirac cone at the Γ point is pseudospin-1 type that is bosonic-like, it is fundamentally different from the fermionic-like Dirac cones at \mathbf{K} and \mathbf{K}' points. They necessarily involve a dispersionless flat band with an infinite effective mass, hosting compact localized states useful for realizing strongly interacting phases of light and matter.^[16,50] However, the phenomena connected with conical diffraction are still quite similar between the Type-B and Type-F Dirac cones, except for the expansion speed. According to Figure 1b, one finds that the first-order derivative of the Type-B Dirac cone is bigger than that of the Type-F Dirac cone.

We present the relating results in **Figure 5a1–a3** and **5b1–b3**. Without any doubt, the beam which excites the state of the Type-B Dirac cone (the blue and green solid squares marked in Figure 2) also expands in the conical diffraction. Comparing with the conical diffraction from Type-F Dirac cone, one can see that the shape of the conical diffraction ring here is a perfect circle without any notches, so that the intensity distribution is not only symmetric about the $x = 0$ but also about the $y = 0$ axis. In addition, the radius of the conical diffraction at a shorter distance $z = 1668$ in Figure 5 is comparable with that at $z = 2780$ in Figure 4. The disappearance of the notch in the conical diffraction is due to the fact that the approximate Dirac cone state includes a pair of Dirac cone states. This is possible, because if ψ_1 and ψ_2 , which can only excite one Dirac cone state, are solutions of this linear system, any linear combination of the two solutions is also a solution.

Another convenient property of our method is its robustness. If a bulk state that is marked with a star, which is close to the Type-B Dirac cone in Figure 2, is launched, it also can excite the

Dirac cone state, and obtained conical diffraction is displayed in Figures 5c1–c3. The reason is that this state is very close to the Dirac state at Γ point, in which the Dirac cone state still occupies a large region. Hence, the conical diffraction can still be observed. In comparison with the ring in Figure 5a1–a3 and 5b1–b3, the ring in Figure 5c1–c3 is not so perfect. If one chooses the bulk state far from the Dirac cone, it will not excite the Dirac cone state during propagation.

In reality, from the intensity profile of the approximate Dirac cone state one can often directly predict whether the conical diffraction rings will possess a notch or not. In Figures 3a1 and 4b1, the incident beams exhibit strip-like profiles along the y direction, while in Figures 3b1 and 4a1, more energy of the incident beams is distributed along the x direction. From such non-circularly symmetric incident beams, the conical diffraction rings will possess notches. In Figure 5a1, b1, one finds that the incident beam is circularly symmetric, so there is no notch in the conical diffraction ring. In Figure 5c1, the incident beam is also non-circularly symmetric, so the conical diffraction ring is not as perfect as that in Figure 5a3, b3.

4. Conclusion

In summary, we have successfully observed conical diffraction in the superhoneycomb lattice, based on the continuous model, through adopting approximate Dirac cone states calculated from the truncated superhoneycomb lattice with short-bearded boundaries. The method we have utilized is direct, accurate, efficient, and easy to follow. We have found conical diffraction from Dirac cones not only at points K and K' but also at the Γ point of the superhoneycomb lattice. Whether the conical diffraction rings possess a notch or not depends on the intensity profiles of the approximate Dirac cone state. If it is circularly symmetric, then there are no notches and the conical diffraction rings are perfect. We believe our research provides a more feasible way to prepare the incident beam and conditions for observing conical diffraction and other interesting topics related to the conical diffraction in real experiments.

Acknowledgements

This work was supported by Natural Science Foundation of Guangdong province (2018A0303130057), National Natural Science Foundation of China (11534008), Ministry of Science and Technology of the People's Republic of China (2016YFA0301404), and Fundamental Research Funds for the Central Universities (xzy012019038, xzy022019076, xjj2017059). Work at TAMUQ is supported by the NPRP 8-028-1-001 project from the Qatar National Research Fund.

Conflict of Interest

The authors declare no conflict of interest.

Keywords

conical diffraction, dirac cone, superhoneycomb lattice

Received: July 2, 2019
Revised: August 10, 2019
Published online: September 5, 2019

- [1] S. Longhi, *Laser Photon. Rev.* **2009**, 3, 243.
- [2] M. C. Rechtsman, J. M. Zeuner, Y. Plotnik, Y. Lumer, D. Podolsky, F. Dreisow, S. Nolte, M. Segev, A. Szameit, *Nature* **2013**, 496, 196.
- [3] L. Lu, J. D. Joannopoulos, M. Soljačić, *Nat. Photon.* **2014**, 8, 821.
- [4] T. Ozawa, H. M. Price, A. Amo, N. Goldman, M. Hafezi, L. Lu, M. C. Rechtsman, D. Schuster, J. Simon, O. Zilberberg, I. Carusotto, *Rev. Mod. Phys.* **2019**, 91, 015006.
- [5] M. I. Katsnelson, K. S. Novoselov, A. K. Geim, *Nat. Phys.* **2006**, 2, 620.
- [6] O. Peleg, G. Bartal, B. Freedman, O. Manela, M. Segev, D. N. Christodoulides, *Phys. Rev. Lett.* **2007**, 98, 103901.
- [7] M. J. Ablowitz, S. D. Nixon, Y. Zhu, *Phys. Rev. A* **2009**, 79, 053830.
- [8] D. Leykam, O. Bahat-Treidel, A. S. Desyatnikov, *Phys. Rev. A* **2012**, 86, 031805.
- [9] F. Diebel, D. Leykam, S. Kroesen, C. Denz, A. S. Desyatnikov, *Phys. Rev. Lett.* **2016**, 116, 183902.
- [10] D. Song, V. Paltoglou, S. Liu, Y. Zhu, D. Gallardo, L. Tang, J. Xu, M. Ablowitz, N. K. Efremidis, Z. Chen, *Nat. Commun.* **2015**, 6, 6272.
- [11] M. Kohmoto, Y. Hasegawa, *Phys. Rev. B* **2007**, 76, 205402.
- [12] O. Bahat-Treidel, O. Peleg, M. Grobman, N. Shapira, M. Segev, T. Pereg-Barnea, *Phys. Rev. Lett.* **2010**, 104, 063901.
- [13] M. C. Rechtsman, Y. Plotnik, J. M. Zeuner, D. Song, Z. Chen, A. Szameit, M. Segev, *Phys. Rev. Lett.* **2013**, 111, 103901.
- [14] V. Apaja, M. Hyrkäs, M. Manninen, *Phys. Rev. A* **2010**, 82, 041402.
- [15] N. Goldman, D. F. Urban, D. Bercioux, *Phys. Rev. A* **2011**, 83, 063601.
- [16] R. A. Vicencio, C. Cantillano, L. Morales-Inostroza, B. Real, C. Mejía-Cortés, S. Weimann, A. Szameit, M. I. Molina, *Phys. Rev. Lett.* **2015**, 114, 245503.
- [17] Z. Lan, N. Goldman, P. Öhberg, *Phys. Rev. B* **2012**, 85, 155451.
- [18] H. Zhong, Y. Q. Zhang, Y. Zhu, D. Zhang, C. B. Li, Y. P. Zhang, F. L. Li, M. R. Belić, M. Xiao, *Ann. Phys. (Berlin)* **2017**, 529, 1600258.
- [19] H. Leblond, B. A. Malomed, D. Mihalache, *Phys. Rev. A* **2011**, 83, 063825.
- [20] Y. Q. Zhang, X. Liu, M. Belić, W. P. Zhong, C. B. Li, H. X. Chen, Y. P. Zhang, *Rom. Rep. Phys.* **2016**, 68, 230.
- [21] T. Jacqmin, I. Carusotto, I. Sagnes, M. Abbarchi, D. D. Solnyshkov, G. Malpuech, E. Galopin, A. Lemaître, J. Bloch, A. Amo, *Phys. Rev. Lett.* **2014**, 112, 116402.
- [22] D. Song, S. Liu, V. Paltoglou, D. Gallardo, L. Tang, J. Zhao, J. Xu, N. K. Efremidis, Z. Chen, *2D Mater.* **2015**, 2, 034007.
- [23] H. Zhong, R. Wang, M. R. Belić, Y. P. Zhang, Y. Q. Zhang, *Opt. Express* **2019**, 27, 6300.
- [24] Y. Zong, S. Xia, L. Tang, D. Song, Y. Hu, Y. Pei, J. Su, Y. Li, Z. Chen, *Opt. Express* **2016**, 24, 8877.
- [25] H. Martin, E. D. Eugenieva, Z. Chen, D. N. Christodoulides, *Phys. Rev. Lett.* **2004**, 92, 123902.
- [26] D. N. Neshev, T. J. Alexander, E. A. Ostrovskaya, Y. S. Kivshar, H. Martin, I. Makasyuk, Z. Chen, *Phys. Rev. Lett.* **2004**, 92, 123903.
- [27] Z. Chen, H. Martin, E. D. Eugenieva, J. Xu, A. Bezryadina, *Phys. Rev. Lett.* **2004**, 92, 143902.
- [28] J. Yang, I. Makasyuk, P. G. Kevrekidis, H. Martin, B. A. Malomed, D. J. Frantzeskakis, Z. Chen, *Phys. Rev. Lett.* **2005**, 94, 113902.
- [29] X. Wang, Z. Chen, P. G. Kevrekidis, *Phys. Rev. Lett.* **2006**, 96, 083904.
- [30] Y. Q. Zhang, M. R. Belić, H. B. Zheng, H. X. Chen, C. B. Li, J. N. Xu, Y. P. Zhang, *J. Opt. Soc. Am. B* **2014**, 31, 2258.

- [31] Y. Sun, D. Leykam, S. Nenni, D. Song, H. Chen, Y. D. Chong, Z. Chen, *Phys. Rev. Lett.* **2018**, *121*, 033904.
- [32] S. Xia, A. Ramachandran, S. Xia, D. Li, X. Liu, L. Tang, Y. Hu, D. Song, J. Xu, D. Leykam, S. Flach, Z. Chen, *Phys. Rev. Lett.* **2018**, *121*, 263902.
- [33] D. Song, D. Leykam, J. Su, X. Liu, L. Tang, S. Liu, J. Zhao, N. K. Efremidis, J. Xu, Z. Chen, *Phys. Rev. Lett.* **2019**, *122*, 123903.
- [34] Y. Plotnik, M. C. Rechtsman, D. Song, M. Heinrich, J. M. Zeuner, S. Nolte, Y. Lumer, N. Malkova, J. Xu, A. Szameit, Z. Chen, M. Segev, *Nat. Mater.* **2014**, *13*, 57.
- [35] J. Noh, S. Huang, K. P. Chen, M. C. Rechtsman, *Phys. Rev. Lett.* **2018**, *120*, 063902.
- [36] J. Noh, W. A. Benalcazar, S. Huang, M. J. Collins, K. P. Chen, T. L. Hughes, M. C. Rechtsman, *Nat. Photon.* **2018**, *12*, 408.
- [37] L. Tarruell, D. Greif, T. Uehlinger, G. Jotzu, T. Esslinger, *Nature* **2012**, *483*, 302.
- [38] G. Jotzu, M. Messer, R. Desbuquois, M. Lebrat, T. Uehlinger, D. Greif, T. Esslinger, *Nature* **2014**, *515*, 237.
- [39] Y. Q. Zhang, Z. K. Wu, M. R. Belić, H. B. Zheng, Z. G. Wang, M. Xiao, Y. P. Zhang, *Laser Photon. Rev.* **2015**, *9*, 331.
- [40] Z. Y. Zhang, F. Li, G. Malpuech, Y. Q. Zhang, O. Bleu, S. Koniakhin, C. B. Li, Y. P. Zhang, M. Xiao, D. D. Solnyshkov, *Phys. Rev. Lett.* **2019**, *122*, 233905.
- [41] Y. V. Kartashov, D. V. Skryabin, *Optica* **2016**, *3*, 1228.
- [42] Y. V. Kartashov, D. V. Skryabin, *Phys. Rev. Lett.* **2017**, *119*, 253904.
- [43] S. Klembt, T. H. Harder, O. A. Egorov, K. Winkler, R. Ge, M. A. Bandres, M. Emmerling, L. Worschech, T. C. H. Liew, M. Segev, C. Schneider, S. Höfling, *Nature* **2018**, *562*, 552.
- [44] Y. Q. Zhang, Y. V. Kartashov, Y. P. Zhang, L. Torner, D. V. Skryabin, *Laser Photon. Rev.* **2018**, *12*, 1700348.
- [45] Y. Q. Zhang, Y. V. Kartashov, Y. P. Zhang, L. Torner, D. V. Skryabin, *APL Photon.* **2018**, *3*, 120801.
- [46] C. Li, F. Ye, X. Chen, Y. V. Kartashov, A. Ferrando, L. Torner, D. V. Skryabin, *Phys. Rev. B* **2018**, *97*, 081103.
- [47] Y. V. Kartashov, D. V. Skryabin, *Phys. Rev. Lett.* **2019**, *122*, 083902.
- [48] Y. Q. Zhang, Y. V. Kartashov, A. Ferrando, *Phys. Rev. A* **2019**, *99*, 053836.
- [49] M. Berry, M. Jeffrey, *Prog. Opt.* **2007**, *50*, 13.
- [50] S. Taie, H. Ozawa, T. Ichinose, T. Nishio, S. Nakajima, Y. Takahashi, *Sci. Adv.* **2015**, *1*, 1500854.